Irreversible versus reversible aggregation: Mean field theory and experiments

ARTICLE *in* THE JOURNAL OF CHEMICAL PHYSICS · OCTOBER 2004

Impact Factor: 2.95 · DOI: 10.1063/1.1779571 · Source: PubMed

6 AUTHORS, INCLUDING:

Gerardo Odriozola
Metropolitan Autonomous University
59 PUBLICATIONS **572** CITATIONS
SEE PROFILE

Artur Schmitt
University of Granada
52 PUBLICATIONS **703** CITATIONS
SEE PROFILE

Jose Callejas-Fernandez
University of Granada
68 PUBLICATIONS **786** CITATIONS
SEE PROFILE

Roque Hidalgo-Alvarez
University of Granada
265 PUBLICATIONS **4,220** CITATIONS
SEE PROFILE

Irreversible versus reversible aggregation: Mean field theory and experiments

G. Odriozola
Programa de Ingeniería Molecular, Instituto Mexicano del Petróleo, Lázaro Cárdenas 152, 07730 México, Distrito Federal, México

R. Leone
Departamento de Química Física y Matemática, Facultad de Química, Universidad de la República, 11800 Montevideo, Uruguay

A. Schmitt, J. Callejas-Fernández, R. Martínez-García, and R. Hidalgo-Álvarez[a)]
Departamento de Física Aplicada, Universidad de Granada, Campus de Fuentenueva, E-18071 Granada, Spain

(Received 22 December 2003; accepted 15 June 2004)

Colloidal aggregation processes arising at different electrolyte concentrations were studied by means of experiments and confronted with theoretical predictions of different kinetic aggregation models. For this purpose, aqueous dispersions of relatively large polystyrene microspheres were chosen as experimental systems. Aggregation was induced by adding KBr electrolyte to the initially stable particle dispersions. During the aggregation processes, the cluster-size distribution was monitored by means of single cluster light scattering. Analyzing the time evolution of the monomer concentration, we found that the processes arising even at moderate electrolyte concentrations cannot be described by pure time-independent irreversible aggregation models. Hence, alternative models such as time-dependent irreversible aggregation and several reversible aggregation models were also tested. The model that considers a time-dependent sticking probability was found to fit the data quite satisfactorily. Nevertheless, the fitted was so slow that it seems not very likely to find such a behavior in real systems. The aggregation-fragmentation models reported in the literature were unable to reproduce the experimental observations. Hence, a more realistic reversible aggregation model was developed. This model accounts also for reenforced or double bonds between the constituent particles. The corresponding fit improved significantly and reached the same quality as the time-dependent model. Moreover, the obtained fitting parameters were in qualitative agreement with the DLVO predictions and so, reversible aggregation seems to be a more reasonable explanation for the experimental data than time-dependent irreversible aggregation. However, no definite statement on the possible secondary bond fragmentation mechanism may be made since both the applied shear stress in the measuring cell and thermal fluctuations can cause weaker bonds to break.
[DOI: 10.1063/1.1779571]

I. INTRODUCTION

Aggregation processes arising in colloidal systems are highly complex. If, for example, a dispersion of sticky hard spheres begins to aggregate, some dimers and a few trimers will have formed almost immediately. Due to the stochastic character of the underlying aggregation mechanisms, however, there might eventually be one pentamer due to a fortuitous collision between a dimer and a trimer. One should realize that monomers, the most mobile specie, are the only ones that show an isotropic diffusive movement. This isotropic character is already lost for aggregates as small as dimers that move faster in the direction parallel to their main axis than perpendicular to it. For larger aggregates, the situation becomes even more complicated since there are not even two trimers of identical shape. Hence, it seems a very ambitious task to model such systems and to develop a theory capable of describing the ongoing processes in reasonable detail. Nevertheless, quite successful efforts have been made in order to describe these ever evolving processes and to overcome all these difficulties with the aid of adequate assumptions and simplifications.[1–9]

The behavior of real aggregation processes, however, may be even more complicated than aggregation of the hard sphere system described above. There might be additional effects such as long range interactions, external fields, reversibility, internal cluster restructuring, charge redistribution, or size and shape inhomogeneities of the constituent particles. Since they may affect the aggregation process they have to be taken into account for a proper description of real systems. Hence, it becomes important to develop strategies capable to identify and distinguish between them. Unfortunately, this is also not expected to be an easy task.

[a)]Electronic mail: rhidalgo@ugr.es

The present work could be seen as an attempt to determine the detailed mechanisms underlying a set of aggregation experiments. Salt-induced aggregation processes were studied by means of experiments and kinetic mean field theories. The experimental systems were chosen to be aqueous dispersions of relatively large polystyrene microspheres, and aggregation was induced using KBr as electrolyte. The time evolution of the cluster-size distributions was monitored by single cluster light scattering (SCLS) and then compared with stochastic solutions of the master equation for several aggregation models. These models may predict either an ever evolving process that finally leads to a single aggregate containing all the particles in the system or give rise to an equilibrium state where the cluster size distribution fluctuates around some average values. Confronting the experimental data with the theoretical predictions of the different models, we expect to elucidate the underlying aggregation mechanisms that are involved.

The paper is organized as follows: Sec. I is the introduction. Section II reviews the theoretical background. The experimental systems and techniques are summarized in Sec. III. In Sec. IV, we show that time-independent irreversible aggregation models fail do describe the experimental data. Section V presents an irreversible aggregation model that considers a time-dependent sticking probability and the corresponding solutions. In Sec. V, the experimental data are compared with the predictions made by some aggregation-fragmentation models reported in the literature. Section VI describes the development of a model based on the idea of reenforced or double bonds. Finally, Sec. VII summarizes the results and extracts the conclusions.

II. THEORETICAL BACKGROUND

The master equation for reversible aggregation processes reads[10–13]

$$\frac{dP(\vec{N},t)}{dt}=\frac{1}{2V}\sum_{i,j}k_{ij}[(N_i+1)(N_j+1+\delta_{ij})P(\vec{N}_{ij}^{+},t)-N_i(N_j-\delta_{ij})P(\vec{N},t)]+\frac{1}{2}\sum_{n=2}^{\infty}\left[(N_n+1)\sum_{i=1}^{n-1}f_{i(n-i)}P(\vec{N}_{i(n-i)}^{-},t)-N_n\sum_{i=1}^{n-1}f_{i(n-i)}P(\vec{N},t)\right], \tag{1}$$

where $P(\vec{N},t)$ is the probability for finding the system in the state $\vec{N}=(N_1,N_2,\ldots,N_n)$ at time t, N_i is the number of i-size particles, k_{ij} is the aggregation kernel, and f_{ij} is the fragmentation kernel. The states $\vec{N}_{ij}^{+}$ and $\vec{N}_{ij}^{-}$ are given by

$$\vec{N}_{ij}^{+}=\begin{cases}(\ldots,N_i+1,\ldots,N_j+1,\ldots,N_{i+j}-1,\ldots) & \text{for } i\neq j\\ (\ldots,N_i+2,\ldots,N_{2i}-1,\ldots) & \text{for } i=j\end{cases},$$

$$\vec{N}_{ij}^{-}=\begin{cases}(\ldots,N_i-1,\ldots,N_j-1,\ldots,N_{i+j}+1,\ldots) & \text{for } i\neq j\\ (\ldots,N_i-2,\ldots,N_{2i}+1,\ldots) & \text{for } i=j\end{cases}.$$

The aggregation rate constants k_{ij} establish the mean rate at which i mers and j mers stick together and form $(i+j)$ mers. Similarly, the fragmentation rate constants f_{ij} denote the mean rate at which $(i+j)$ mers break into i mers and j mers. Both, the aggregation and the fragmentation kernels have to be understood as orientational and configurational averages of the exact aggregation and fragmentation rates.

The algorithms used in this work for solving Eq. (1) for a particular aggregation and fragmentation kernel are essentially a combination of the standard procedures described in the literature for solving the master equation for pure aggregation and pure fragmentation processes.[14–16] The exact details are described in previous works.[10–13]

Expression (1) models irreversible diffusion-limited cluster aggregation (DLCA) if one sets $f_{ij}=0$ and uses the Brownian kernel

$$k_{ij}^{Brown}=\tfrac{1}{4}k_{11}(i^{1/d_f}+j^{1/d_f})(i^{-1/d_f}+j^{-1/d_f}) \tag{2}$$

as aggregation kernel. Here, k_{11} is the dimer formation rate constant and d_f is the cluster fractal dimension. The Brownian kernel describes aggregation processes where all cluster and particle collisions lead to bond formation, i.e., it assumes the sticking probability to be unity.

When the clusters still diffuse freely but react on contact with a given sticking probability P, the situation changes and two reacting clusters may perform several consecutive collisions before they finally stick together or eventually diffuse away. In this case, the Brownian kernel has to be modified in order to account for these noneffective collisions. In previous work we showed that the corresponding aggregation kernel is given by

$$k_{ij}^{irr}=\frac{k_{ij}^{Brown}P\mathcal{N}_{11}(ij)^b}{(1+P[\mathcal{N}_{11}(ij)^b-1])}, \tag{3}$$

where $\mathcal{N}_{11}$ is the average number of consecutive collisions per encounter for nonaggregating monomers and b is a constant exponent.[17] The numerical values of $\mathcal{N}_{11}$ and b were determined by means of simulations to be $\mathcal{N}_{11}=6.1$ and $b=0.35$ for the simulation conditions used in Refs. 10, 17, and 18. It should be noted that the aggregation kernel given by

Eq. (3) models irreversible aggregation of noninteracting particles for any sticking probability. It is time independent and includes the limiting case of DLCA and reaction limited cluster aggregation for $P=1$ and $P\to 0$, respectively.

In the literature, we reported on several relatively simple kernels for cluster breakup.[10,11] One of the proposed fragmentation kernels reads

$$f_{ij}=e_{ij}(1+\delta_{ij})(1-P_{Cij})/\tau_b, \tag{4}$$

where τ_b is the characteristic decay time of an exponentially shaped bond breakup probability density function and P_{Cij} is the probability for two recently produced fragments to collide and reaggregate immediately. We showed that $1-P_{Cij}$ can be approximated by $[\mathcal{N}_{11}(ij)^b]^{-1}$. The function e_{ij} represents the average number of bonds contained in the n-sized clusters that, on breakup, lead to i- and j-size fragments. It was obtained in Ref. 10 for loopless aggregates and parametrized by the following fitted expression:

$$e_{ij}(1+\delta_{ij})=p_1(i^{p_2}+j^{p_2})(i^{p_3}+j^{p_3})(ij)^{p_4}, \tag{5}$$

where $p_1=0.4391$, $p_2=1.006$, $p_3=-1.007$, and $p_4=-0.1363$ for the used simulation conditions.

It should be noted that the combined use of expressions (2) and (4) as aggregation and fragmentation kernels in the master equation models a system where all collisions lead to bond formation and the produced bonds live an average time τ_b. In other words, it models a Lennard-Jones-type particle interaction potential. Frequently found particle interaction potentials in colloids, however, are usually characterized by a very deep minimum on close contact, followed by an energetic barrier at short distances, and a shallow secondary minimum. The width and depth of the secondary minimum depend on the particular system. Considering that primary bonds are irreversible, the following fragmentation kernel was proposed for this type of potentials:

$$f_{ij}=\frac{e_{ij}(1+\delta_{ij})(1-P_{Cij})E_2}{(E_1+E_2)\tau_{b2}}, \tag{6}$$

where the number of primary and secondary bonds are denoted as E_1 and E_2, respectively. τ_{b2} is the average secondary bond lifetime. Furthermore, a primary bond formation probability P_1 had to be introduced in the algorithm in order to decide whether a primary or a secondary bond is formed when a cluster-cluster collision occurs. Please note that this model includes pure irreversible aggregation as a limiting case for $\tau_{b2}\to 0$. Evidently, a bond lifetime approaching zero means that the formed bonds break immediately and so, the preceding cluster-cluster collision can be safely considered as noneffective. In other words, this limiting case implies that all cluster-cluster collisions in the secondary minimum are noneffective while cluster-cluster collisions in the primary minimum always give rise to the formation of irreversible bonds. Consequently, the primary bond formation probability P_1 plays the role of a sticking probability. In order to check this equivalency, we calculated the corresponding stochastic solution of the master equation and compared the obtained results with the solutions obtained for the pure irreversible model, i.e., using expression (3) as aggregation kernel and $f_{ij}=0$ as fragmentation kernel. Since the obtained agreement was excellent we may safely claim that the proposed reversible aggregation model contains the irreversible model as a limiting case.

Finally, if the primary bonds are also allowed to break, the fragmentation kernel becomes

$$f_{ij}=\frac{e_{ij}(1+\delta_{ij})(1-P_{Cij})}{(E_1+E_2)}\left[\frac{E_1}{\tau_{b1}}+\frac{E_2}{\tau_{b2}}\right], \tag{7}$$

where τ_{b1} denotes the primary bond lifetime. Please note that the latter fragmentation kernels are implicitly time dependent since they are functions of the evolving numbers of primary and secondary bonds present in the system. This implies, of course, that the time evolution of the entire systems depends also on the bond populations. Consequently, E_1 and E_2 have to be included in the state vector and the master equation has to be modified accordingly. This yields

$$\begin{aligned}\frac{dP(\vec{M},t)}{dt}=&\frac{1}{2V}\sum_{i,j}k_{ij}\{(N_i+1)(N_j+1+\delta_{ij})[P(\vec{M}_{ij}^{+1},t)P_1+P(\vec{M}_{ij}^{+2},t)(1-P_1)]-N_i(N_j-\delta_{ij})P(\vec{M},t)\}\\&+\frac{1}{2}\sum_{n=2}^{\infty}\left[(N_n+1)\sum_{i=1}^{n-1}f_{i(n-i)}[P(\vec{M}_{i(n-i)}^{-1},t)P_{b1}+P(\vec{M}_{i(n-i)}^{-2},t)(1-P_{b1})]-N_n\sum_{i=1}^{n-1}f_{i(n-i)}P(\vec{M},t)\right]\\&+\frac{1}{2}\sum_{n=2}^{\infty}N_n\sum_{i=1}^{n-1}\frac{f_{i(n-i)}P_{Ci(n-i)}}{1-P_{Ci(n-i)}}[P(\vec{M}^{*1},t)P_{b1}(1-P_1)+P(\vec{M}^{*2},t)(1-P_{b1})P_1\\&-P(\vec{M},t)(P_{b1}(1-P_1)+(1-P_{b1})P_1)],\end{aligned} \tag{8}$$

where $P(\vec{M},t)$ is the probability for finding the system in the state $\vec{M}=(N_1,N_2,\ldots,N_n,E_1,E_2)=(\vec{N},E_1,E_2)$ at time t and $P_{b1}=E_1/\tau_1(E_1/\tau_1+E_2/\tau_2)$ is the probability that a given fragmentation event breaks a primary bond. The displaced states $\vec{M}_{ij}^{+1}$, $\vec{M}_{ij}^{+2}$, $\vec{M}_{ij}^{-1}$, $\vec{M}_{ij}^{-2}$, $\vec{M}^{*1}$, and $\vec{M}^{*2}$ are given by

$$\vec{M}_{ij}^{+1}=(\vec{N}_{ij}^{+},E_1-1,E_2),$$

$$\vec{M}_{ij}^{+2}=(\vec{N}_{ij}^{+},E_1,E_2-1),$$

$$\vec{M}_{ij}^{-1}=(\vec{N}_{ij}^{-},E_1+1,E_2),$$

$$\vec{M}_{ij}^{-2}=(\vec{N}_{ij}^{-},E_1,E_2+1),$$

$$\vec{M}^{*1}=(\vec{N},E_1+1,E_2-1),$$

$$\vec{M}^{*2}=(\vec{N},E_1-1,E_2+1).$$

Please note that formation and fragmentation of primary and secondary bonds are now considered as different events. The additional right-hand term accounts for those changes in the bound population that leave the cluster-size distribution unaltered. This happens, for example, when a secondary bound breaks and the fragments reaggregate immediately forming a primary bond. The stochastic algorithm used for solving the modified master equation is described in Ref. 11 although Eq. (8) is not explicitly written there. In this equation it is clearly seen how the obtained solutions contain the time evolution of the detailed cluster-size distribution and the bond populations.

III. EXPERIMENTAL PROCEDURES

Aggregation processes arising in aqueous suspensions of polystyrene microspheres were measured by means of SCLS. The polystyrene particles were manufactured at the laboratories of Granada University without any added surface active agents following the procedure described by Goodwin *et al.*[19] The particles are charge stabilized by sulfate groups deriving from the initiator molecules used for the polymerization reaction. The particle size and shape were checked by transmission electron microscopy. The obtained average mean particle diameter and polydispersity index were (630 ± 4) nm and 1.004, respectively. The surface charge density, as determined by conductimetric titration, was (-54 ± 2) mC/m^2.

The single cluster light scattering instrument used for the study allows the time evolution of the cluster-size distribution to be monitored up to heptamers. Its principle of operation is based on hydrodynamic focusing of the aggregating sample which means that sample is injected very slowly into a faster flowing water stream. Consequently, the sample flow narrows and the distance between the clusters contained therein increases. The sample flow containing the separated clusters is then forced to cross a focused laser beam. If the cluster concentration is sufficiently low, the clusters pass the laser focus individually. As they cross, they scatter a pulse of light which is detected at a small scattering angle. Under these conditions, the scattered light pulse intensity is directly related to the cluster size and so, a detailed cluster-size distribution can be obtained by simply counting the pulses as a function of their intensity. Further details of the experimental technique can be found in previous works.[20,21] It should be mentioned that hydrodynamic focusing exerts stress on the aggregates and some bonds might eventually break. Pelssers *et al.* however, showed that the hydrodynamic forces are several orders of magnitude smaller than the binding forces for particles aggregated at high electrolyte concentration.[22] Moreover, they also estimated possible changes of the cluster-size distribution due to additional orthokinetic aggregation in the apparatus to be negligible. This means that the applied shear stress cannot break the stronger bonds formed in the deep primary energy minimum. Weaker bonds formed in the relatively shallow secondary energy minimum, however, may eventually be broken. Therefore, we will not be able to make definite statements about the reason for weaker bond breakup and both fragmentation mechanisms, thermal fluctuations and shear stress in the measuring cell, may take place.

Prior to the experiments, the samples were diluted to twice the desired particle concentration and sonicated for 10 min in order to approach monomeric initial conditions. Immediately afterwards, the aggregation process was started by mixing equal volumes of sample and electrolyte solution through a Y-shaped mixing device. The mixture remained unstirred in the reaction vessel during the entire aggregation process. At equally spaced time intervals, samples were drawn automatically and injected into the measuring cell for size analysis. The initial particle concentration in the reaction vessel was set to 1.0×10^{14} m^{-3} in order to guarantee proper detection of individual aggregates. Sedimentation was not observed. The electrolyte concentrations were 500, 250, 125, and 63 mM potassium bromide (KBr). The temperature was stabilized at (20 ± 1) °C. The pure water used for the experiments was obtained by reverse osmosis followed by percolation through charcoal and a mixed bed of ion-exchange resins. The initial cluster-size distribution was measured for a stable, electrolyte free sample. The fraction of particles associated in doublets was always below 0.3% in the initial suspension. Larger aggregates were not detected.

IV. DO AGGREGATES PERFORM SPONTANEOUS BREAKUP?

It is well known that the classical Deryaguin-Landau-Vervey-Overbeck (DLVO) theory predicts the existence of a secondary minimum of finite depth for the interaction potential of two colloidal particles. The depth of the predicted minimum increases with increasing particle size so that it is expected to keep two sufficiently large particles together once the particle size has reached a critical value. This effect is shown in Fig. 1 where the potential energy is calculated using the following DLVO potential:

$$V_{el}=2\pi\varepsilon_r\varepsilon_0(a+\delta)\Psi_S^2\ln\{1+\exp[-\kappa(H-2\delta)]\},$$

$$V_{vdW}=-\frac{A}{6}\left[\frac{2a^2}{H(4a+H)}+\frac{2a^2}{(2a+H)^2}+\ln\left(\frac{H(H+4a)}{(2a+H)^2}\right)\right],$$

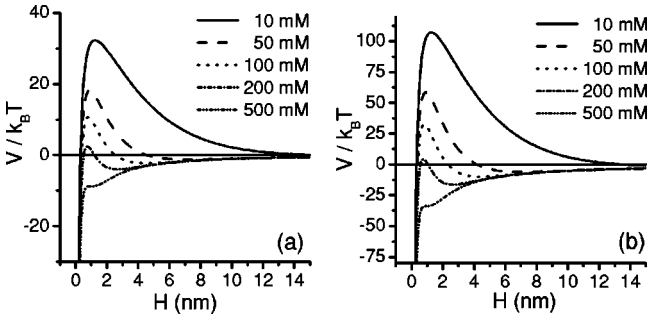

FIG. 1. Potential energy calculated by means of Eq. (9) for a monovalent symmetric electrolyte. The considered particle radii were $a=92$ nm (a) and $a=315$ nm (b). The remaining parameters are the same in both plots. The different curves correspond to the electrolyte concentrations indicated in the plots.

$$V_{DLVO}=V_{el}+V_{vdW}. \tag{9}$$

Here, V_{el} and V_{vdW} are the electric and London–van der Waals contributions to the total DLVO potential V_{DLVO}. δ and Ψ_S are the thickness and the potential of the Stern layer. a is the particle radius and H is the distance between the particle surfaces. κ is the reciprocal Debye length and A is the Hamaker constant. For the curves shown in Fig. 1, the following typical values were assumed: $\Psi_0=-15.0$ mV, $T=20\,^{\circ}$C, $A=3.0\times10^{-21}$ J, $\delta=0.133\times10^{-9}$ m.

As was already mentioned before, the curves show a primary and a secondary minimum separated by an energetic barrier. The height of this energy barrier decreases with increasing electrolyte concentration. The secondary minima can keep the particles together only if their depth is at least several thermal energies k_BT. This is clearly the case for almost all the interparticle potential curves of the larger particles shown in Fig. 1. The finite depth of the secondary minima supports the idea of possible spontaneous bond breakup. Nevertheless, breakup of weaker bonds may also occur due to the stress exerted on the aggregates in the measuring apparatus. Unfortunately, the experimental data presented in this paper will not allow us to distinguish between these two possible fragmentation mechanisms. We will comment on this aspect at the end of this paper.

Before we try to use reversible aggregation models for the description of our experimental data, the existence of cluster breakup should be confirmed. For that purpose, the time evolution of the monomer concentration was analyzed. Figures 2(a), 2(b), 2(c), and 2(d) show these curves for the experimental systems aggregating at 500, 250, 125, and 63 mM KBr, respectively. The solid and the dashed lines in this figure represent the corresponding solution of the master equation for the Brownian kernel and for the kernel

$$k_{ij}^{fit}=\begin{cases}k_{11} & i=j=1\\ 0 & \text{otherwise,}\end{cases}$$

respectively. Both kernels were fitted only to the onset of the aggregation processes. The fractal dimension in the Brownian kernel was fixed to the typical DLCA value of 1.75. The dimer formation rate constant k_{11} was used as a common fitting parameter for both kernels. As expected, the Brownian kernel fits the data very well at high electrolyte concentration for $k_{11}=6.0\times10^{-18}$ m^3/s. This value falls well into the range of $k_{11}=(6\pm3)\times10^{-18}$ m^3 s^{-1}, determined by Sonntag and Strenge for diffusion-limited cluster aggregation.[23] The excellent agreement between the fit and the data is even maintained for all aggregation times [see Fig. 2(a)]. This is not surprising since very similar results were obtained for the same particles aggregating at 1000 mM KBr.[24] At lower electrolyte concentrations, the good agree-

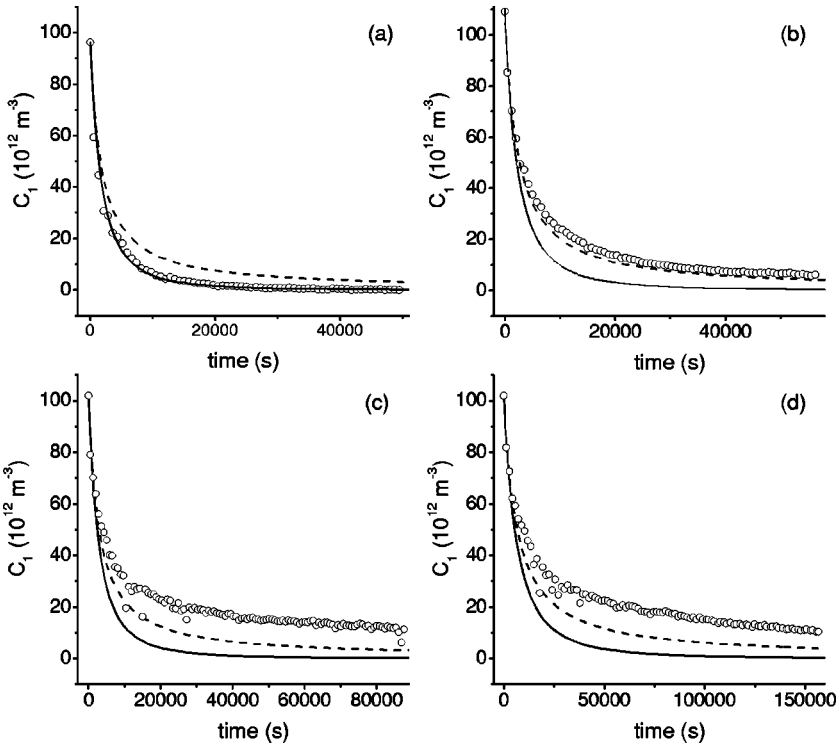

FIG. 2. Time evolution of the monomer concentration for systems aggregating at (a) 500, (b) 250, (c) 125, and (d) 63 mM KBr. The symbols correspond to the experimental data while the solid and dashed lines show the solutions of the master equation for the Brownian kernel and for the slowest possible irreversible aggregation kernel k_{ij}^{fit}, respectively.

ment is lost as the aggregation process proceeds. The kernel k_{ij}^{fit} represents the slowest possible decrease for monomers arising in pure irreversible aggregation processes since it allows the monomers only to react among themselves generating just dimers. Evidently, the experimental monomer concentrations drop immediately below this limiting case at high electrolyte concentration. At low electrolyte concentrations, however, the experimental monomer concentrations remain always above this slowest case of time-independent irreversible aggregation [see Figs. 2(b)–2(d)]. This seems to indicate that monomers are generated from larger aggregates and so, aggregate breakup should be taking place. For both kernels, the fitted dimer formation rate constants k_{11} were 6.0, 4.0, 3.5, and 1.5×10^{-18} m^3/s for 500, 250, 125, and 63 mM KBr, respectively. The values obtained for the lower electrolyte concentrations are quite high if compared with typical values reported for slow aggregation processes.[23] Taking into account that the classical DLVO theory does not predict any potential barrier at distances larger than the position of the secondary minimum, it seems reasonable to assume that all cluster collisions lead necessarily to bond formation in the secondary minimum and only a small fraction of the colliding clusters overcomes the energy barrier forming strong primary bonds. If the secondary bonds have a relatively short but nonvanishing lifetime, a higher aggregation rate would be detected.

Unfortunately, this is not the only explanation one might evoke. Lin *et al.* suggested that the cluster reactivity of slowly aggregating small polystyrene beads could change with time due to an increase in the energy barrier.[25] This means that the entire aggregation kernel could be time dependent. Possible explanations for a slowdown of the aggregation rates are partial coalescence, charge and residual surfactant redistribution, rearrangement of short polymer chains not bonded to the particle core, changes of the particles roughness due to a change of the electrolyte concentration, among others. These possible effects, however, involve entities much smaller than the comparatively huge colloidal particles used in this study. Hence, the corresponding time scales are expected to be much smaller than the measured aggregation times.

Since the aggregation processes under investigation are more likely to be of reversible nature, they should be compared with the solutions of the master equation for the different fragmentation kernels presented in Sec. II. Notwithstanding, it seems interesting to check at least to which extent time-dependent aggregation kernels can reproduce the experimental data. This will be done in the following section.

V. COMPARISON WITH TIME-DEPENDENT KERNELS

As previously mentioned, a possible explanation for a slowdown of the aggregation processes is that the potential barrier between polystyrene particles may increase during aggregation. This implies that the sticking probability P and the corresponding aggregation kernels decrease in time. To the best of our knowledge, there is no known analytic expression for the time dependence of $P(t)$ or $k_{ij}(t)$. Since the physical phenomena supporting the idea of a time-dependent aggregation kernel imply some kind of reaccommodation or relaxation processes in the system, we propose to use an exponential time dependence like $P(t)=P_\infty+(P_0-P_\infty)\exp(-ct^{1/2})$. In this equation, P_0 and P_∞ are the sticking probabilities for $t=0$ and $t\to\infty$, respectively. Parameter c gives the decay rate for the underlying physical process. Time-dependent irreversible aggregation is then modeled using the proposed time-dependent sticking probability $P(t)$ in the irreversible aggregation kernel given by Eq. (3) and setting $f_{ij}=0$. Please note that this irreversible aggregation model assumes implicitly that the clusters diffuse freely and react on contact with a time-dependent sticking probability. This means that cluster diffusion is not affected by the changing sticking probability and so, the Brownian part of the irreversible aggregation kernel should be the same for all electrolyte concentrations. This is why we used the dimer formation rate constant as a single fitting parameter for the complete set of experimental data while the parameters P_0, P_∞, and c that affect the probability part were allowed to vary freely for either electrolyte concentration. The values obtained for P_0, P_∞, and c are summarized in Table I. The fitted dimer formation rate constant was $k_{11}=7.5\times10^{-18}$ m^3/s. This value differs from the previously fitted value of 6.0×10^{-18} m^3/s since it is not only monomers that were considered in the fit. Nevertheless, it still falls perfectly within the interval given by Sonntag and Strenge for experimental diffusion limited cluster aggregation.[23]

TABLE I. Parameters P_0, P_∞, and c used to fit the experimental data.

[KBr] (mM)	P_0	P_∞	c ($s^{-1/2}$)
500	1	1	⋯
250	0.21 ± 0.03	0.008 ± 0.002	0.020 ± 0.004
125	0.14 ± 0.02	0.004 ± 0.001	0.020 ± 0.004
63	0.05 ± 0.01	0.003 ± 0.001	0.014 ± 0.003

The experimental data together with the best fits are plotted in Fig. 3. As can be seen, the fitted lines reproduce the data quite satisfactorily. The obtained time constants, however, correspond to relaxation times of the order of hours. This does not seem to be very reasonable since most possible relaxation-type processes taking place in the samples are expected to occur on a much shorter time scale. Furthermore, also the hypothesis of partial coalescence made by Lin *et al.* can be ruled out. We checked by means of transmission electron microscopy that our relatively large polystyrene particles remain perfectly spherical even when they form large aggregates.

Hence, we conclude that it is possible to reproduce the experimental data using time-dependent irreversible aggregation models. Nevertheless, the obtained fitting parameters are not very reasonable and so, we will now proceed to compare the experimental data with reversible aggregation models.

VI. COMPARISON WITH KNOWN REVERSIBLE AGGREGATION MODELS

Figure 4 shows the experimental data of the time evolution of the cluster-size distribution up to heptamers and of

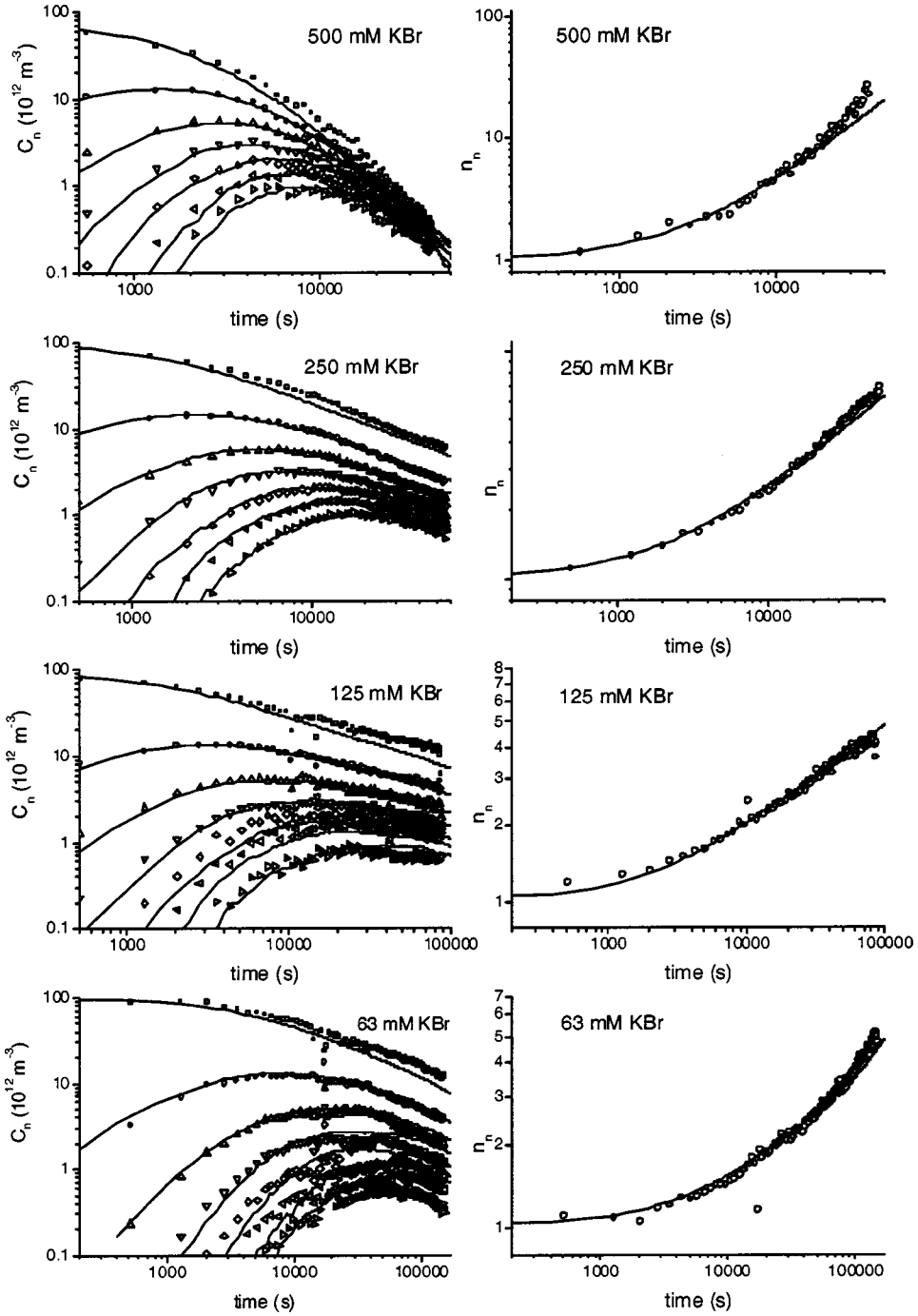

FIG. 3. Time evolution of the cluster size distribution, $C_n(t)$, and the number average cluster size, $n_n(t)$, obtained at different electrolyte concentrations. The symbols (□), (○), (△), (▽), (◇), (◁), and (▷) in the left-hand plots represent the experimental results for monomers up to heptamers, respectively. The lines show the stochastic solutions obtained considering the time-dependent sticking probability $P(t)=P_\infty+(P_0-P_\infty)\exp(-ct^{1/2})$ in the irreversible aggregation kernel given by Eq. (3).

the number average cluster size arising at 63 mM KBr. The discussion starts with the data obtained at the lowest electrolyte concentration since it is here where fragmentation, if present, is expected to be more abundant. The continuous lines in Fig. 4 represent the best fit obtained using τ_b as a fitting parameter for the fragmentation kernel given by Eq. (4). The Brownian kernel was employed as aggregation kernel since, in the present model, all cluster-cluster collisions are considered to lead to bond formation. All stochastic solutions were calculated using the following parameters: $N_0=50\,000$, $V=5.0\times10^{-10}$ m^3, $k_{11}=6.0\times10^{-18}$ m^3 s^{-1}, $d_f=2.0$, $N_{11}=6.1$, and $b=0.35$. The relatively large number of particles, N_0, is necessary to ensure reasonably good statistics. The reaction volume V was fixed so that the particle concentration equals that of the experiments. The dimer formation rate constant k_{11} in the Brownian aggregation kernel was set to the same value used in Sec. IV since this value was shown to model the fast aggregating system quite satis-

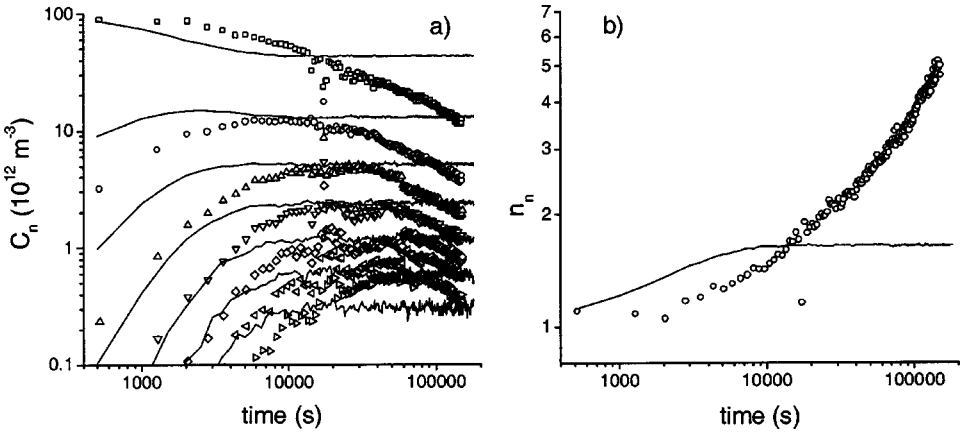

FIG. 4. Time evolution of the cluster size distribution $C_n(t)$ (a), and the number average cluster size $n_n(t)$ (b) arising at 63 mM KBr. The symbols (□), (○), (△), (▽), (◇), (◁) and (▷) in plot a) correspond to monomers up to heptamers, respectively. The lines show the stochastic solution obtained by fitting τ_b in Eq. (4).

factorily. The fractal dimension was taken to be that usually found for fragmentation processes. Due to the lack of experimental data for N_{11} and b, the values obtained by computer simulation were used for the fits.

As can be seen in Fig. 4, the obtained fit is very poor. This is not surprising since the fitted kernel corresponds to an aggregation-fragmentation model where only one type of reversible bonds is allowed. In other words, the corresponding particle interaction potential shows only one finite minimum at short distances and so, differs quite strongly from the expected DLVO potentials shown in Fig. 1. Moreover, the fitted curves reach an equilibrium state that is not observed for the ever evolving experimental data.

In order to improve the fits, we now consider the fragmentation kernel given by Eq. (6). This kernel considers not only breakable secondary bonds but also unbreakable primary bonds. Figure 5 shows the best fit using the primary bond formation probability P_1 and the secondary bond lifetime τ_{b2} as freely adjustable parameters. Since also here all collisions are expected to lead to bond formation, the aggregation kernel k_{ij} is kept unchanged. τ_{b2} has to be small to ensure a proper fit of the onset of the aggregation process. Hence, the long time behavior was fitted by changing mainly P_1. The best fit was obtained for $P_1=0.025$ and $\tau_{b2}=75$ s. As can be observed in Fig. 5, the corresponding curves clearly describe the experimental data much better than before. Nevertheless, serious discrepancies remain that are most pronounced at long aggregation times. There, the cluster-size distribution evolves slower than the theoretical predictions. This may indicate that also the primary bonds should be considered to be breakable.

Figure 6 compares the experimental data with the predictions obtained using expression (7) as fragmentation kernel. This kernel considers the possibility of primary bond breakup but, unfortunately, introduces the primary bond lifetime τ_{b1} as an additional freely adjustable parameter. Since τ_{b1} affects only the long time behavior of the cluster-size distribution, the previously fitted parameters were maintained for keeping the good agreement at short and intermediate times. Hence, we tried to fit the long time behavior by changing τ_{b1}. The best fit was obtained for $\tau_{b1}=2\times10^5$ s. It should be emphasized that very few primary bond breakup events change the long time behavior of the predicted curves quite considerably. As observed in Fig. 6, the fitted curves are now much closer to the experimental data. The relatively high value obtained for τ_{b1} seems to be quite reasonable for primary bonds that are expected to be hardly breakable.

Although the fit has improved quite substantially, it is

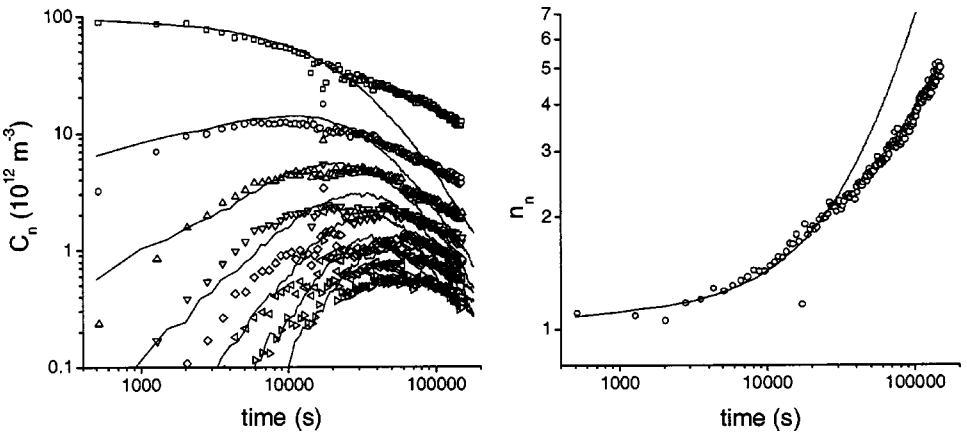

FIG. 5. The experimental data shown in Fig. 4 but now compared with the stochastic solution obtained by fitting P_1 and τ_{b2} in Eq. (6).

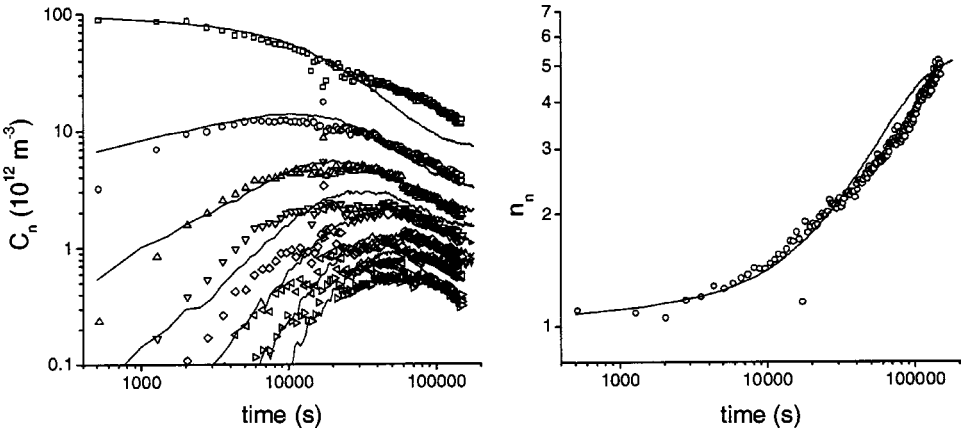

FIG. 6. The experimental data shown in Fig. 4 but now compared with the stochastic solution obtained by fitting P_1, τ_1, and τ_2 in Eq. (7).

still not very satisfactory for two major reasons: (a) there are still some discrepancies mainly at long times and (b) the final tendency is not matched. The latter point is clearly observable for the time evolution of the number average cluster size n_n. Furthermore, it is quite evident that the deviations from the experimental curves are expected to increase if one tries to extrapolate the fitted curve for even longer times. One should bear in mind that this aggregation-fragmentation model predicts a long time equilibrium state which does not seem to be an adequate description for our set of experimental data.

Ending this section, we would like to conclude that none of the three fitted fragmentation kernels is capable to fit the experimental data satisfactorily. This implies that if reversible aggregation is taking place there are additional effects that are not accounted for in those models. In other words, if pure reversible aggregation is responsible for the experimental observations, it involves more details than only the formation of breakable primary and secondary bonds. Unless those effects are identified and included in the theoretical description, only poor fits will be obtained.

VII. A FURTHER ATTEMPT

Due to the lack of a theoretical fragmentation model that fits our experimental data satisfactorily, we will try a further attempt to describe them. This approach is based on some ideas expressed by Pefferkorn and Widmaier.[26] These authors propose three different bonding mechanisms. The first mechanism is the one we have considered up to now. It occurs when a pair of constituent particles of two colliding aggregates get into contact and form a single bond. The second aggregation mechanism takes place when an individual particle of one cluster collides simultaneously with two particles of another aggregate. In this way, double bonds may be formed or the single bond formed between the two individual particles of the involved clusters may be at least reenforced by the presence of the third particle. From now on, we will refer to this type of bonds simply as double or reenforced bonds. Evidently, the formation of double bonds becomes possible as soon as the first dimers appear in the system. The third mechanism involves simultaneous aggregation in different zones of the reacting clusters, i.e., several bonds are formed in different areas leading to looplike structures.

These ideas are very intuitive and reasonable and so, the problem lies not in their theoretical foundation but in how to implement them in a kinetic aggregation-fragmentation model. In this section we present an attempt for taking the second mechanism into account. For this purpose, certain assumptions will be made in order to be able to solve the corresponding stochastic master equation. Further effects such as internal cluster rearrangement will not be considered.

Before we tackle the aggregation of clusters of all possible sizes, we first discuss the simplest possible case of monomer-dimer collisions. The number of collisions that lead to single or double bonds can be assumed to be proportional to the dimer surface area A_s and A_d capable to form single or double bonds, respectively. Consequently, the ratios P_s and P_d of single and double bond forming collisions is given by $P_s=A_s/A_t$ and $P_d=A_d/A_t$, where $A_t=A_s+A_d$ is the total available bonding area. Naturally, $P_s+P_d=1$ is satisfied.

Figure 7(a) shows a monomer (particle 1) in simultaneous close contact with both constituent particles of a dimer (particles 2 and 3). In this case, a perfect double bond is established. Figure 7(b) depicts the limiting configuration where the monomer remains in close contact with only one particle of the dimer but still interacts with the other particle. It is just between these two limiting positions, where the 1-2 bond is considered to be reenforced by the presence of particle 3. The dimer regions where bonding is not possible are indicated in Fig. 7(a) as dark patches on the dimer. The brighter areas show the dimer surface regions where bond formation is possible. Only the relatively small strip of the latter region shown in Fig. 7(b) is available for double bonding. For a dimer, the total accessible bonding area is $A_t=2(2\pi a^2\int_0^{2\pi/3}\sin\theta d\theta)=6\pi a^2$. This means that the area $2\pi a^2$ is lost for binding in each particle-particle bond. The available area for double bonds may be determined as $A_d=2(2\pi a^2\int_{2\pi/3-\Delta\theta}^{2\pi/3}\sin\theta d\theta)$ where $\Delta\theta=2\arcsin[(2a+\Delta a)/4a]-\pi/3$ is the angular width of the double bonding area. It is convenient to define $\gamma=\int_{2\pi/3-\Delta\theta}^{2\pi/3}\sin\theta d\theta$ so that A_d becomes $A_d=4\pi a^2\gamma$. This means that γ gives the fraction of the monomer particle surface where reenforced

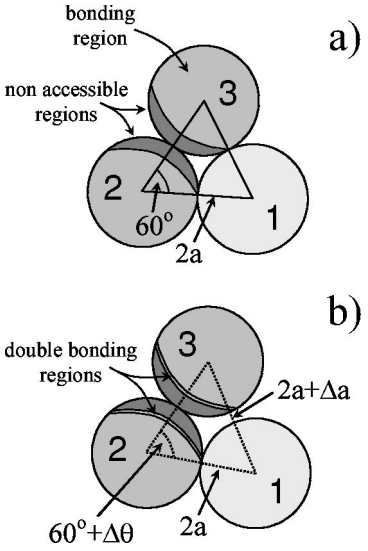

FIG. 7. Schematic view of a monomer (particle 1) reacting with both constituent particles of a dimer (particles 2 and 3). Plot (a) shows the third particle in close contact with both constituent particles while plot (b) depicts particle 3 at the maximum distance where bond reenforcement due to the presence of particle 1 may still be considered.

double bonds may be formed. Assuming that the particle-particle interaction has a cutoff length of 10% of the particle radius, i.e., $\Delta a=0.1a$, yields $\gamma=0.051\,25$, $P_d=A_d/A_t=0.034\,17$, and $P_s=A_s/A_t=0.965\,83$.

In order to extend the previous ideas to the collision of any pair of i- and j-size clusters, we assume the fraction of collisions that give rise to single bonds to be proportional to the probability of finding a single bonding spot on either cluster. Accordingly, the fraction of collisions that lead to double bond formation should be proportional to the probability of finding a double bonding surface patch on cluster i and a single bonding patch on cluster j and vice versa. This yields

$$P_s=\frac{A_s}{A_t}\bigg|_i\frac{A_s}{A_t}\bigg|_j,$$

$$P_d=\frac{A_d}{A_t}\bigg|_i\frac{A_s}{A_t}\bigg|_j+\frac{A_s}{A_t}\bigg|_i\frac{A_d}{A_t}\bigg|_j,$$

$$P_{dd}=\frac{A_d}{A_t}\bigg|_i\frac{A_d}{A_t}\bigg|_j, \tag{10}$$

where P_{dd} represents the probability for a collision to occur between two double bonding areas. The areas in the former equations can be estimated as follows for loopless clusters made of n constituent particles:

$$A_t|_n=n4\pi a^2-(n-1)2\pi a^2=(n+1)2\pi a^2,$$

$$A_d|_n=(n-1)4\pi a^2\int_{2\pi/3-\Delta\theta}^{2\pi/3}\sin\theta d\theta=(n-1)4\pi a^2\gamma,$$

$$A_s|_n=A_t|_n-A_d|_n. \tag{11}$$

Taking into account that the probability for a collision between two double bonding areas is expected to be extremely small, P_{dd} may be safely neglected. This yields finally for the fractions of single and double bond forming collisions,

$$P_s=1-P_d,$$

$$P_d=\frac{2\gamma(i-1)}{(i+1)}\left[1-\frac{2\gamma(j-1)}{(j+1)}\right]+\frac{2\gamma(j-1)}{(j+1)}\left[1-\frac{2\gamma(i-1)}{(i+1)}\right]. \tag{12}$$

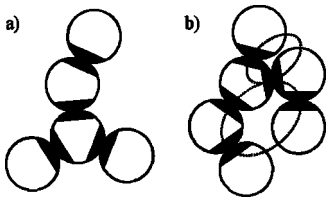

FIG. 8. Two-dimensional projection of two aggregates, one without (a) and another with (b) overlapping regions and steric impediments. The sterically not accessible regions are indicated by means of dashed lines.

This approach assumes implicitly that there is no overlap of areas where bond formation cannot take place. Furthermore, it neglects the possibility that steric impediments might block the access to some parts of a given aggregate. Figure 8 shows the two-dimensional projection of two aggregates, one with and another without overlapping regions and steric impediments. It should be emphasized that steric impediments deny the access to entire parts of the aggregates that include single, double, and nonbonding regions. Hence, this effect is not expected to alter the estimations of expression (12) substantially. The overlap of nonaccessible regions, however, leads to an underestimation of the total available bonding area and an overestimation of the cluster surface available for double bonds. Hence the cluster surface available for single bonds will be underestimated since it is calculated as the difference between the total bonding area and the double bonding area. Moreover, if there are overlapping double bonding areas, P_d would be also overestimated. Nevertheless, the effect of overlapping of not accessible regions and double bonding regions cannot be very pronounced since the clusters form relatively open and branched structures. Bearing these limitations in mind, we will use the expressions given in Eq. (12) as a reasonable approximation. Please note that these expressions are symmetric with respect to i and j. Furthermore, they establish $P_d=0$ for $i=j=1$, $P_i\simeq 4\gamma-8\gamma^2$ for $i,j\to\infty$, $P_i\to 2\gamma$ for $i=1$, $j\to\infty$ or $j=1$, $i\to\infty$. Assuming γ to be ≈ 0.05, the values of P_d lie within the interval of $[0,\,4\gamma]=[0,\,0.2]$. In other words, the fraction of double bond forming collisions never exceeds 20%, which seems to be quite reasonable.

So far, the proposed model establishes that a given collision has a probability P_d for leading to a reenforced bond and a probability P_s for single bonding. The model, however, should also take into account that both single and double bonds can be formed in the primary or secondary energy minimum, according to the primary bond formation probability P_1. Since the primary particle-particle interaction energy minimum is usually quite deep, we will assume that all primary bonds are irreversible, no matter whether they are single or double in nature. Hence, single and double primary

bonds are characterized by an infinite lifetime, $\tau_{1s}=\tau_{1d}=\infty$, while single and double secondary bonds have a finite lifetime τ_{2s} and τ_{2d}, respectively. In this way, only three free parameters remain although we had to introduce further but quite reasonable assumptions.

For this model, the fragmentation kernel reads finally

$$f_{ij}=\frac{e_{ij}(1+\delta_{ij})(1-P_{Cij})}{(E_{1s}+E_{2s}+E_{1d}+E_{2d})}\left[\frac{E_{2s}}{\tau_{2s}}+\frac{E_{2d}}{\tau_{2d}}\right], \tag{13}$$

where E_{1s} and E_{2s} are the populations of primary and secondary single bonds and E_{1d} and E_{2d} are the populations of primary and secondary double bonds, respectively. Evidently, only two kinds of bonds contribute to the proposed fragmentation kernel. It should be mentioned that this fragmentation kernel seems to be almost identical with the one given by Eq. (7). However, the main difference lies not in the analytical form of the fragmentation kernel but in the corresponding master equation that should now consider formation and breakup of the four different types of bonds. It would be quite tedious and not very instructive to report this lengthy equation here and so, we prefer to comment on the algorithm employed for solving it. The flow diagram of the solving algorithm is shown in Fig. 9. It starts with an initialization step where the cluster and bond populations are set to their initial values and the reaction channels are calculated accordingly. Immediately afterwards, the main aggregation-fragmentation loop is entered. Here, the reaction time τ the cluster sizes and the reaction type are obtained just as explained in Ref. 11. In case of aggregation, the cluster size distribution is updated and three random numbers homogeneously distributed in [0,1] are generated and compared with P_d and P_1. This is done in order to decide which bond type will be formed. Similarly, when secondary bond breakup occurs, a further random number is generated and compared with $(E_{2s}/\tau_{2s})/(E_{2s}/\tau_{2s}+E_{2d}/\tau_{2d})$ in order to determine whether a single or a double secondary bond has to be broken. Finally, a further random number controls whether reaggregation takes place or not. The main loop finishes when a single aggregate containing all the system particles is obtained.

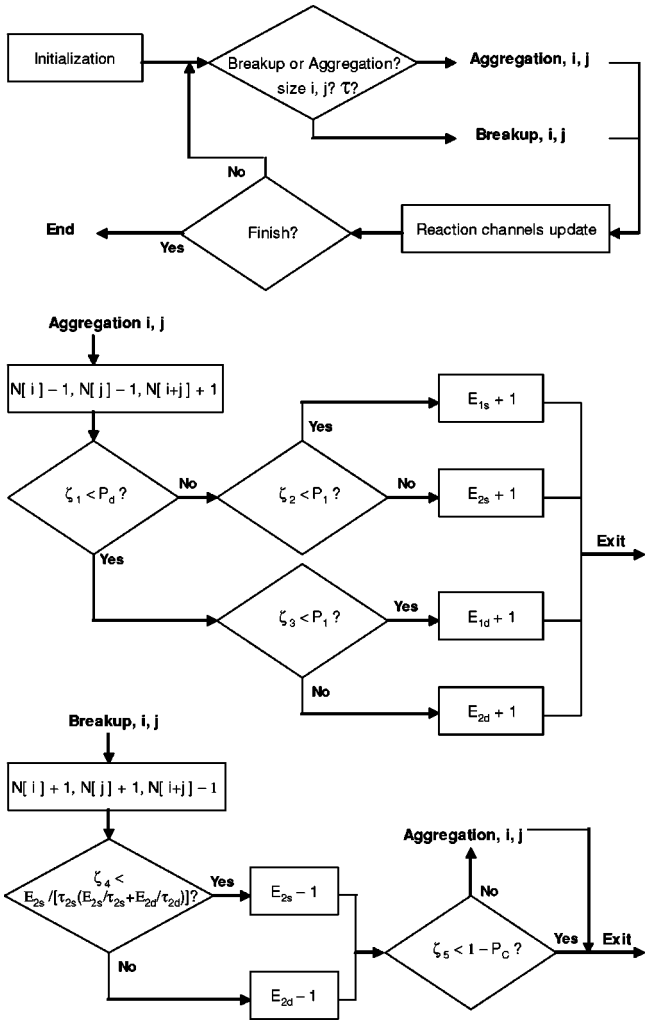

FIG. 9. Flow diagram of the solving procedure for the master equation considering the formation of primary and secondary single bonds and primary and secondary double bonds.

Figure 10 shows the time evolution of the cluster size distribution and the corresponding number average cluster size for all different KBr concentrations. The symbols correspond to the experimental data. The lines represent the stochastic solution obtained by means of the algorithm described in this section. As done in Sec. V, the dimer formation rate constant k_{11} was used as a single fitting parameter for the complete set of experimental data while only three fitting parameters where allowed to vary freely for either electrolyte concentration. The obtained results for the used fitting parameters P_1, τ_{2s}, and τ_{2d} are summarized in Table II. The fitted dimer formation rate constant was $k_{11}=9.0\times10^{-18}$ m^3/s. This value gives the best fits here and, although it differs from the previously fitted values, still falls within the interval given by Sonntag and Strenge for experimental diffusion limited cluster aggregation.[23]

As already shown in Fig. 3 and Table I, the 500 mM KBr data set is reasonably well matched by a pure DLCA model. This means, evidently, that the potential barrier has completely disappeared as predicted by the classical DLVO theory. So, it may seem unnecessary to refit the data using a reversible model. It is included here just for the sake of completeness since the reversible aggregation model gives exactly the same results as the DLCA model if one sets $P_1=1.0$ or τ_{2s} and $\tau_{2d}\rightarrow\infty$. Hence, the relatively large values obtained for P_1, τ_{2s}, and τ_{2d} confirm the DLCA-like behavior and the tiny improvement gained by the use of the three free fitting parameters is by no means justified in this particular case.

According to Fig. 10, a clear improvement of the fits with respect to the former reversible aggregation models is observed. Moreover, the long time tendencies are now reproduced much more satisfactorily. This is true not only for the cluster-size distribution but also for the number average cluster size at all electrolyte concentrations. Hence, it becomes clear that an aggregation-fragmentation model that considers reenforced double bonds describes the experimental data much better. Nevertheless, some minor discrepancies between the stochastic solutions and the experimental data still remain. These remaining discrepancies, however, suggest that additional effects such as multiple particle contacts, loop

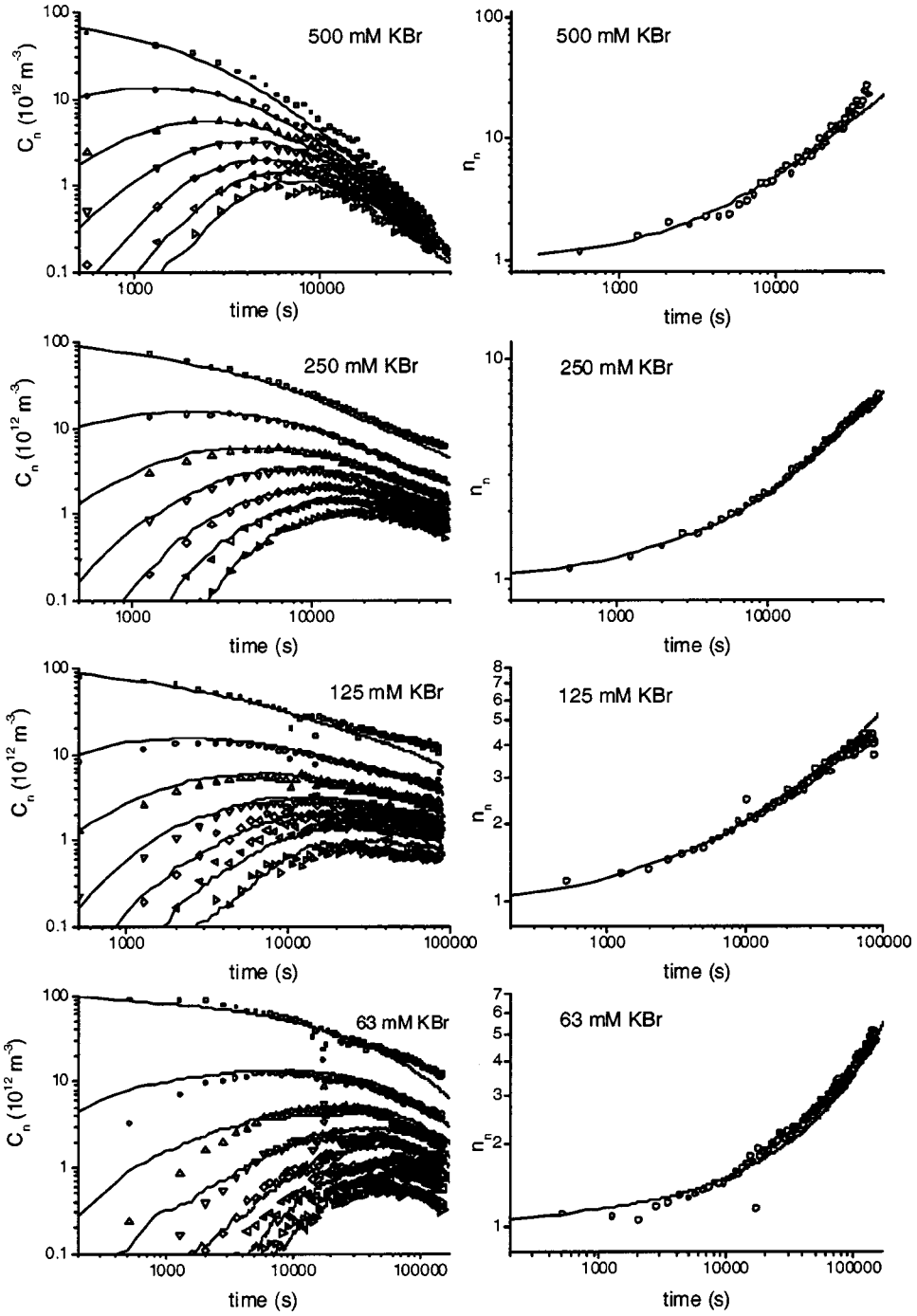

FIG. 10. The same experimental data as presented in Fig. 3. The lines show the stochastic solutions obtained by fitting P_1, τ_{2s}, and τ_{2d}, in Eq. (13).

formation or even cluster rearrangement might be present. These effects are expected to play a major role only for larger aggregates and so, τ_{2d} should be the most affected parameter by the fact of not considering them.

Before we start to interpret the obtained results, we would like to point out that the proposed model has more free parameters than we would like it to have. We tried hard to keep this number at least as low as the number of freely adjustable parameters used for the time-dependent irreversible model fitted in Sec. V. This is why we started comparing our experimental data with the simplest possible models. Since the results were not satisfactory, further and more complex models had to be developed. Consequently, additional effects had to be included leading inevitably to an increased number of free parameters. Furthermore, additional assumptions had to be made in order to keep the deduced aggregation-fragmentation kernel as simple as possible. These assumptions, although reasonable, limit the validity of the results. Hence, the fitted values of P_1, τ_{2s}, and τ_{2d} should be taken with care while their relative values deserve more confidence, since all made assumptions were kept the same in all cases.

As can be seen in Table II, the primary bond formation probability P_1 increases with increasing electrolyte concen-

TABLE II. Parameters P_1, τ_{2s}, and τ_{2d} used to fit the experimental data. The errors were estimated from the sensibility of the fitted solutions.

[KBr] (mM)	P_1	τ_{2s} (s)	τ_{2d} (s)
500	0.54 ± 0.08	350 ± 150	9000 ± 3000
250	0.033 ± 0.006	200 ± 70	8000 ± 3000
125	0.010 ± 0.003	140 ± 60	6000 ± 2500
63	0.007 ± 0.004	30 ± 20	3500 ± 2000

tration. Since P_1 should be inversely related with the height of the energetic barrier that separates the primary from the secondary minimum, it can be concluded that the barrier height is also inversely related to the electrolyte concentration. Furthermore, the lifetime of the single and double secondary bonds increases for increasing electrolyte concentration. Hence, the same should be true for the depth of secondary minimum. All these experimental observations are in qualitative agreement with the shape of the particle interaction potentials predicted by the classical DLVO theory (see Fig. 1). The fact that the double secondary bonds are characterized by very long lifetimes is not surprising since they are reenforced due to the simultaneous interaction between three particles.

Figure 11 shows the theoretical predictions of the time evolution of the different bond types for the 63 mM KBr case. As can be seen, the fraction of the different bond types changes quite dramatically with time. At the beginning of the aggregation process, most of the collisions lead to single secondary bonds. Due to their short lifetime, they start to break and the number of double secondary bonds surpasses their population. Once the aggregation time reaches the average lifetime of the double secondary bonds, they begin to break and their concentration finally diminishes. At this point, the number of unbreakable primary bonds becomes important. These results are quite reasonable and in good agreement with the experimental work performed by Pefferkorn and Widmaier.[26]

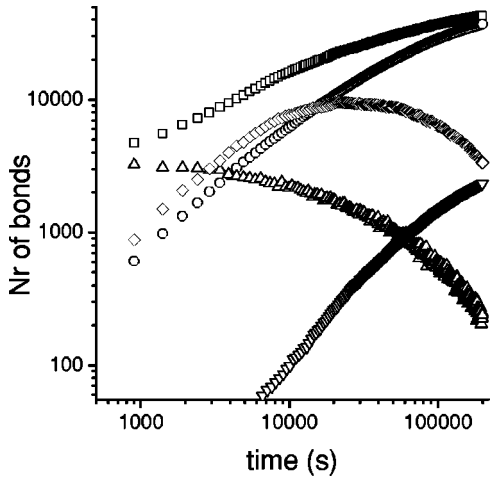

FIG. 11. Time evolution of the total number of bonds (□), single primary (○), single secondary (△), double primary (▽), and double secondary bonds (◇), obtained by means of the stochastic algorithm. The parameters used for the solution correspond to the fit of the experimental data obtained at 63 mM KBr.

Ending this section, we would like to comment on the possibility of additional cluster breakup due to hydrodynamic focusing. If some bonds broke due to the exerted stress and if the fragments separated enough before passing through the laser beam, the measured cluster size distribution would have an extra contribution of smaller clusters and a lack of larger ones. The extent of this contribution, if any, is not known. In the worst case, all fragmentation processes would be produced by the exerted shear stress. This, however, seems not very likely since the applied stress is certainly not strong enough to break the primary bonds formed at high electrolyte concentration. Only the weaker bonds formed in the shallow secondary minimum could be broken by shear. Nevertheless, even if all the weaker bonds broke due to hydrodynamic focusing, the measured curves would be evolving in time due to the ongoing formation of stronger bonds. Hence, the models presented here would be still useful to analyze the data, since τ_{2s} and τ_{2d} parametrize the bond strength, although the absolute values would be somehow altered due to the additional cluster breakup.

VIII. CONCLUSIONS

The time evolution of the cluster-size distribution and the number average cluster size were observed by means of single cluster light scattering. Aqueous suspensions of polystyrene microspheres were used as experimental systems. Aggregation was induced adding different amounts of KBr electrolyte.

Several aggregation-fragmentation models already reported in the literature were used to fit the data. Since the results were not satisfactory, a further model was developed. This model includes the possibility of multiple particle contacts that give rise to reenforced or double bonds. This idea was previously proposed in Ref. 26. The proposed model improves the fit of the experimental data quite substantially. The obtained fitting parameters are in qualitative agreement with the shape of the particle interaction potentials predicted by the classical DLVO theory.

Furthermore, a time-dependent irreversible aggregation model was also tested. Therefore, an exponentially relaxing sticking probability was assumed in the irreversible aggregation kernel. Its results also lead to a good agreement with the experimental data. The fitted decay times, however, are so long that is seems unlikely to find such slow relaxation processes in the samples. Nevertheless, their existence cannot be excluded and both time-dependent irreversible aggregation and reversible aggregation might even take place simultaneously. Hence, more experimental information is required to clearly elucidate the underlying aggregation mechanism.

One possibility would be to perform experiments at different volume fractions. Since aggregation kinetics is second order and breakup is first order, significant differences are expected. However, the narrow range of concentrations that our single particle light scattering instrument can handle makes this a quite difficult task. The possible cluster breakup due to hydrodynamic focusing within the apparatus limits the significance of these measurements even further. Notwithstanding, forced cluster breakup could even be helpful for

distinguishing between different bonding strengths that might be present in the aggregates. If the clusters break in the apparatus, a time correlation between the larger and smaller clusters is expected. This could be, in principle, also detected with our single particle light scattering instrument. Nevertheless, the present controlling software does not allow us to measure these time correlations. We hope to implement this possibility in the near future.

Finally, we think that the existence of weak bonds and cluster breakup seems more likely and reasonable than a relatively slow increase of the potential energy barrier during aggregation. This opinion is supported by the DLVO theory that predicts shallower secondary minima for smaller particles. Consequently, such particles will form secondary bonds with shorter lifetimes that will break almost immediately. As mentioned before, this is the same as considering the cluster-cluster collision to be noneffective. Hence, it should be possible to model slow aggregation of smaller particles by means of pure irreversible aggregation models. This is exactly what we found in a previous work[27] and indicates that size matters as is qualitatively predicted by the DLVO theory. On the other hand, if an increasing potential barrier were responsible for a slowdown of the overall aggregation rate, it should also take place for the smaller particles. In other words, if phenomena such as rearrangement of charge distribution or rearrangement of nonbonded short polymer chains occur for large particles and this explained the increase of the potential barrier, why should they not occur for smaller colloidal particles as well?

In summary, this study confirms the complex nature of slow aggregation processes and supports the idea of weak bonds and many body contacts within the formed aggregates.

ACKNOWLEDGMENTS

This research was supported by Instituto Mexicano del Petróleo, Grant No. D.00072, and by the Ministerio de Ciencia y Tecnología [Plan Nacional de Investigación Científica, Desarrollo e Innovación Tecnológica (I+D+I), Project No. MAT2003-08356-C04-01].

[1] M. von Smoluchowski, Phys. Z. **17**, 557 (1916).
[2] M. von Smoluchowski, Z. Phys. Chem. **92**, 129 (1917).
[3] P. G. J. van Dongen and M. H. Ernst, J. Stat. Phys. **37**, 301 (1984).
[4] D. A. Weitz and M. Oliveria, Phys. Rev. Lett. **52**, 1433 (1984).
[5] M. Y. Lin, H. M. Lindsay, D. A. Weitz, R. C. Ball, R. Klein, and P. Meakin, Nature (London) **339**, 360 (1989).
[6] M. Y. Lin, R. Klein, H. M. Lindsay, D. A. Weitz, R. C. Ball, and P. Meakin, Phys. Rev. A **41**, 2005 (1990).
[7] M. L. Broide and R. J. Cohen, Phys. Rev. Lett. **64**, 2026 (1990).
[8] M. Lattuada, P. Sandkuhler, H. Wu, J. Sefcik, and M. Morbidelli, Adv. Colloid Interface Sci. **103**, 33 (2003).
[9] G. Odriozola, M. Tirado-Miranda, A. Schmitt, and J. Callejas-Fernández, in *Encyclopaedia of Surface and Colloid Science*, edited by A. Hubbard (Dekker, New York, 2004).
[10] G. Odriozola, A. Schmitt, Moncho-Jordá, J. Callejas-Fernández, R. Martínez-García, R. Leone, and R. Hidalgo-Álvarez, Phys. Rev. E **65**, 031405 (2002).
[11] G. Odriozola, A. Schmitt, J. Callejas-Fernández, R. Martínez-García, R. Leone, and R. Hidalgo-Álvarez, J. Phys. Chem. B **107**, 2180 (2003).
[12] G. Odriozola, A. Schmitt, Moncho-Jordá, J. Callejas-Fernández, R. Martínez-García, R. Leone, and R. Hidalgo-Álvarez, Phys. Rev. E **68**, 069903 (2003).
[13] G. Odriozola, A. Schmitt, J. Callejas-Fernández, R. Martínez-García, R. Leone, and R. Hidalgo-Álvarez, J. Phys. Chem. B **107**, 14145 (2003).
[14] M. Thorn and M. Seesselberg, Phys. Rev. Lett. **72**, 3622 (1994).
[15] M. Thorn, M. L. Broide, and M. Seesselberg, Phys. Rev. E **51**, 4089 (1995).
[16] D. T. Gillespie, J. Phys. Chem. B **81**, 2340 (1977).
[17] G. Odriozola, A. Moncho-Jordá, A. Schmitt, J. Callejas-Fernández, R. Martínez-García, and R. Hidalgo-Álvarez, Europhys. Lett. **53**, 797 (2001).
[18] A. Moncho-Jordá, G. Odriozola, F. Martínez-López, A. Schmitt, and R. Hidalgo-Álvarez, Eur. Phys. J. E **5**, 471 (2001).
[19] J. W. Goodwin, J. Hearn, C. C. Ho, and R. H. Ottewill, Colloid Polym. Sci. **252**, 464 (1974).
[20] A. Fernández-Barbero, M. A. Cabrerizo-Vílchez, R. Martínez-García, and R. Hidalgo Álvarez, Phys. Rev. E **53**, 4981 (1996).
[21] A. Fernández-Barbero, A. Schmitt, M. A. Cabrerizo-Vílchez, and R. Martínez-García, Physica A **230**, 53 (1996).
[22] E. G. M. Pelssers, M. A. Cohen Stuart, and G. J. Fleer, J. Colloid Interface Sci. **137**, 362 (1990).
[23] H. Sonntag and K. Strenge, *Coagulation Kinetics and Structure Formation* (Plenum, New York, 1987).
[24] G. Odriozola, A. Schmitt, J. Callejas-Fernández, R. Martínez-García, and R. Hidalgo-Álvarez, J. Chem. Phys. **111**, 7657 (1999).
[25] M. Y. Lin, H. M. Lindsay, D. A. Weitz, R. C. Ball, R. Klein, and P. Meakin, Nature (London) **339**, 360 (1989).
[26] E. Pefferkorn and J. Widmaier, Colloids Surf. **145**, 25 (1998).
[27] G. Odriozola, M. Tirado-Miranda, A. Schmitt, F. Martínez-López, J. Callejas-Fernández, R. Martínez-García, and R. Hidalgo-Álvarez, J. Colloid Interface Sci. **240**, 90 (2001).